The Set1 complex is dimeric and acts with Jhd2 demethylation to convey symmetrical H3K4 trimethylation

Rupam Choudhury,[1] Sukhdeep Singh,[1] Senthil Arumugam,[2] Assen Roguev,[1,3] and A. Francis Stewart[1]

[1]Genomics, Biotechnology Center, Center for Molecular and Cellular Bioengineering, University of Technology Dresden, 01307 Dresden, Germany; [2]European Molecular Biology Laboratory Australia Node for Single Molecule Science, ARC Centre of Excellence in Advanced Molecular Imaging, School of Medical Sciences, University of New South Wales, Sydney 2052, Australia; [3]Department of Cellular and Molecular Pharmacology, University of California at San Francisco, San Francisco, California 94518, USA

Epigenetic modifications can maintain or alter the inherent symmetry of the nucleosome. However, the mechanisms that deposit and/or propagate symmetry or asymmetry are not understood. Here we report that yeast Set1C/COMPASS (complex of proteins associated with Set1) is dimeric and, consequently, symmetrically trimethylates histone 3 Lys4 (H3K4me3) on promoter nucleosomes. Mutation of the dimer interface to make Set1C monomeric abolished H3K4me3 on most promoters. The most active promoters, particularly those involved in the oxidative phase of the yeast metabolic cycle, displayed H3K4me2, which is normally excluded from active promoters, and a subset of these also displayed H3K4me3. In wild-type yeast, deletion of the sole H3K4 demethylase, Jhd2, has no effect. However, in monomeric Set1C yeast, Jhd2 deletion increased H3K4me3 levels on the H3K4me2 promoters. Notably, the association of Set1C with the elongating polymerase was not perturbed by monomerization. These results imply that symmetrical H3K4 methylation is an embedded consequence of Set1C dimerism and that Jhd2 demethylates asymmetric H3K4me3. Consequently, rather than methylation and demethylation acting in opposition as logic would suggest, a dimeric methyltransferase and monomeric demethylase cooperate to eliminate asymmetry and focus symmetrical H3K4me3 onto selected nucleosomes. This presents a new paradigm for the establishment of epigenetic detail.

[*Keywords*: chromatin; epigenetics; histone demethylation; histone methylation; promoter architecture]

Supplemental material is available for this article.

Received November 2, 2018; revised version accepted February 15, 2019.

The fundamental unit of eukaryotic chromatin, the nucleosome, is composed of four histone pairs (H2A, H2B, H3, and H4) symmetrically arranged around a dyad axis (Luger et al. 1997). Consequentially, it has been naturally presumed that nucleosomes in chromatin are symmetrical. However, high-resolution epigenetic mapping has identified asymmetric distributions of posttranslational modifications and histone variants within nucleosomes near transcription start sites (TSSs). In particular, bivalent nucleosomes with histone 3 Lys27 (H3K27) bimethylation or trimethylation (me2/me3) on one H3 tail and H3K4me3 or H3K36me3 on the other, as well as asymmetric distribution of H4K20me1, have been identified in mammalian cells (Voigt et al. 2012; Shema et al. 2016). In yeast, asymmetric distributions of H3K9ac and H2A.Z indicate new subtleties in promoter architecture (Rhee et al. 2014; Ramachandran et al. 2015). Asymmetric nucleosomes clearly have the potential to contribute to the regulation of, or convey directional orientation within chromatin. To date, very few studies have explored the mechanisms that convey epigenetic symmetries or asymmetries. In the course of studies on the structure of the Set1 complex, Set1C, which is the sole H3K4 methyltransferase in *Saccharomyces cerevisiae*, we unexpectedly encountered this issue.

Among the circuitries involved in epigenetic regulation, H3K4 methylation is one of the most widely conserved. In all eukaryotes, H3K4me3 on promoter nucleosomes is a binding site for protein complexes involved in launching transcription from active promoters including TFIID (Vermeulen et al. 2007, 2010). Furthermore, the size of the H3K4me3 peak equates with the quantity of mRNA produced (Howe et al. 2017; Soares et al. 2017). Nevertheless, the function of the H3K4 methylation system remains

Corresponding author: francis.stewart@tu-dresden.de
Article published online ahead of print. Article and publication date are online at http://www.genesdev.org/cgi/doi/10.1101/gad.322222.118.

enigmatic and no unifying regulatory explanation has emerged (Howe et al. 2017; Woo et al. 2017). This is due to several conundrums including (1) its apparent dispensability for transcription in yeast (Lenstra et al. 2011; Margaritis et al. 2012; Weiner et al. 2012) and *Drosophila* (after somatic mutagenesis) (Hödl and Basler 2012), (2) the counterintuitive finding that loss of H3K4 methylation in yeast provokes more increased than decreased mRNA expression (Margaritis et al. 2012; Weiner et al. 2012), and (3) rather than central transcriptional functions, in higher eukaryotes the H3K4 methyltransferases are only required for very specialized developmental roles (Ernst et al. 2004; Glaser et al. 2009; Lee et al. 2013; Bledau et al. 2014).

The identification of H3K4 demethylases has compounded the enigma. H3K4me2/3 can be removed by the Jarid1/Kdm5 class of Jumonji domain demethylases (Klose et al. 2006; Liang et al. 2007; Huang et al. 2010). Deletion of the only *S. cerevisiae* H3K4 demethylase, Jhd2, has very little effect on gene expression (Ramakrishnan et al. 2016). Similarly, functional studies on the four mouse Jarid1 genes (Kdm5a–d) are confusing because ablation reveals incompletely penetrant and variegating phenotypes (Catchpole et al. 2011; Schmitz et al. 2011; Kidder et al. 2014; Scandaglia et al. 2017).

The eight-subunit yeast Set1 complex, Set1C, was the first H3K4 methyltransferase complex to be biochemically defined (Roguev et al. 2001). It was also described as the seven-subunit COMPASS (complex of proteins associated with Set1) (Miller et al. 2001), with the missing subunit and in vitro H3K4 enzymatic proof added later (Krogan et al. 2002). Set1C/COMPASS is centered on a four-membered subcomplex composed of two heteromeric interactions between Swd1/Swd3 and Bre2/Sdc1 (Roguev et al. 2001; South et al. 2010; Avdic et al. 2011; Tremblay et al. 2014). This subcomplex is the highly conserved scaffold for all Set1/Trithorax-type H3K4 methyltransferases and is now termed WRAD (Ernst and Vakoc 2012) after the mammalian homologs WDR5, RBBP5, ASH2L, and DPY30 (corresponding to Swd3, Swd1, Bre2/Ash2, and Sdc1 in yeast).

Dpy30 was first identified as a protein required for dosage compensation in *Caenorhabditis elegans* (Hsu et al. 1995). When we found a Dpy30 homolog in Set1C (Roguev et al. 2001), we noted that Dpy30 homologs include a region similar to the dimerization interface of the regulatory subunit RIIa of protein kinase A, which is composed of two α helices that form a four-helix bundle during dimerization (Newlon et al. 1999). We proposed that yeast Set1C is dimeric with the Dpy30 homolog, Sdc1, as the dimer interface (Roguev et al. 2003; Dehé et al. 2006). Structural studies with peptides confirmed that the RIIa homology region in DPY30 dimerizes to form an X bundle nearly identical to the dimerization/docking (D/D) domain of PKA RIIa (Wang et al. 2009; Tremblay et al. 2014; Zhang et al. 2015a).

Despite these indications, the contribution of the Dpy30/Sdc1 dimerization interface to the structure and function of H3K4 methyltransferases has not been investigated, possibly because Dpy30 is not required for enzyme activity in vitro (Dou et al. 2005; Li et al. 2016), although inclusion of Dpy30 stimulates activity (Jiang et al. 2011). Here we show that yeast Set1C is dimeric and dimerization relies on the Dpy30/Sdc1 dimer interface. Using alanine mutagenesis of the dimer interface, we observed dramatic changes in H3K4 methylation profiles in yeast strains expressing mutant monomeric Set1C compared with wild type. Insight into the H3K4 methylation profiles was further revealed by deletion of the sole H3K4 demethylase, Jhd2. These findings present a new paradigm for the mechanics of H3K4 methylation and demethylation in eukaryotic epigenetic regulation. Furthermore, our findings extend the recent insights acquired from the high-resolution structures of the monomeric Set1C/COMPASS enzymatic core (Hsu et al. 2018; Qu et al. 2018).

Results

Set1C dimerization is mediated by Sdc1

To evaluate whether Sdc1 contributes to multimerization of Set1C, we used size exclusion chromatography (SEC) to examine the complex with and without Sdc1. Wild-type (wt) Set1C is ~1000 kDa (Miller et al. 2001; Roguev et al. 2003; Trésaugues et al. 2006); however, Set1C lacking Sdc1 is ~400 kDa (Fig. 1A–C). Two discrete *sdc1* mutations, either to delete the Dpy-30 homology box (*sdc1*$^{\Delta 121-165}$) completely or point mutate critical residues within it (*sdc1**; V129A, L133A, L134A) (Fig. 1A; Supplemental Fig. S1A), which were chosen according to previous dimerization mutations in RIIa (Newlon et al. 1999), also reduced the apparent size of Set1C to 400 kDa.

Because Sdc1 interacts with Bre2 (Roguev et al. 2001; South et al. 2010; Tremblay et al. 2014), we evaluated Set1C lacking Bre2 and found that it was also smaller (Fig. 1C), which is consistent with our previous findings that Set1C lacking Bre2 also lacks Sdc1, and vice versa, but all other subunits remain (Dehé et al. 2006). As expected, complete loss of Sdc1 or deletion of the entire Dpy-30 box, which includes the Bre2 interaction site (South et al. 2010; Tremblay et al. 2014), resulted in concomitant loss of Bre2. However, the *sdc1** triple point mutation, which retains the Bre2 interaction site in the Dpy-30 box, retained Bre2 in Set1C (Fig. 1D). Therefore, the Sdc1 dimerization interface and not Bre2 is required for the apparent dimerization of Set1C. These *sdc1* mutations did not alter the expression level of Set1 (Fig. 1E) or the association of any other Set1C subunit except Bre2 (Dehé et al. 2006). Notably, because loss of Spp1 alters the H3K4 methylation profile (Morillon et al. 2005; Dehé et al. 2006), we specifically confirmed that Spp1 is retained in the mutant *sdc1* Set1Cs (Supplemental Fig. S1B).

Two further tests for Set1C dimerization were used. First, we made a yeast strain expressing two different tagged versions of Set1: TAP-Set1 and Myc-Set1. Immunoprecipitation using the TAP tag also retrieved Myc-Set1 (Fig. 1F), demonstrating that wild-type Set1C includes more than one copy of Set1. Second, we used fluorescence correlation spectroscopy (FCS) and photon counting histogram (PCH) for direct quantitation of Set1C stoichiometry in whole-cell extracts. FCS-PCH measures photon counts

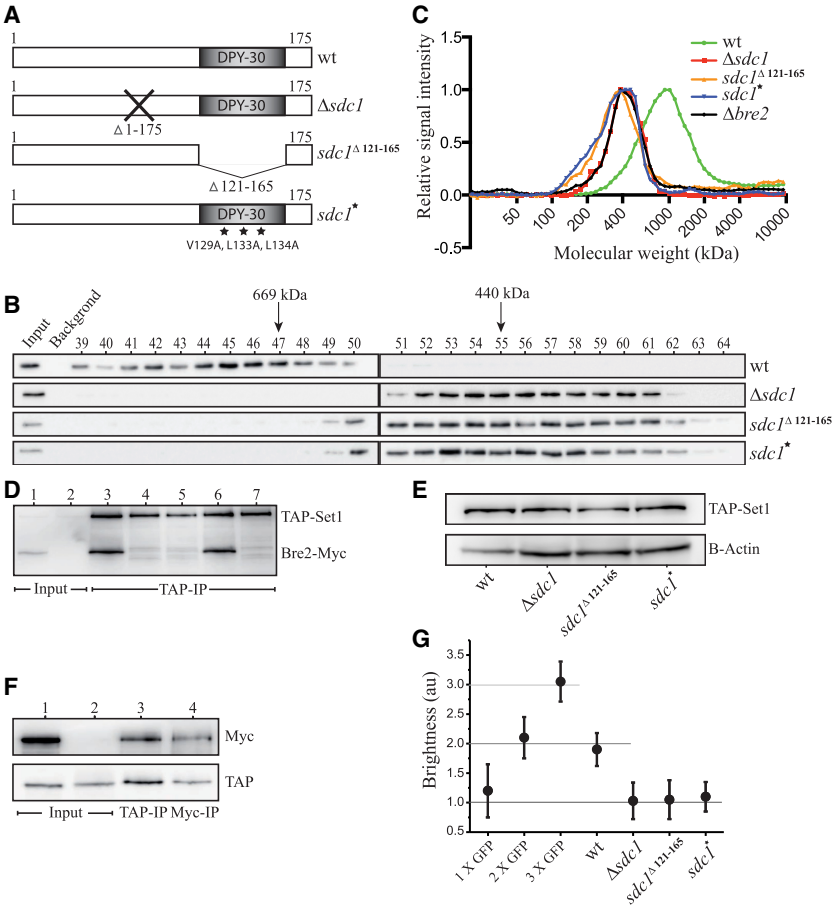

Figure 1. The DPY30 domain of Sdc1 mediates the dimerization of Set1C. (*A*) Schematic representation of Sdc1 and Sdc1 mutants used in the study showing the conserved DPY-30 box that includes the RIIa dimerization interface that was deleted (Δ121–165) or point mutated (V129A, L133A, L134A). (*B*) SEC on Superose 6 columns of total TAP-Set1 cell extracts from the indicated strains. The columns were calibrated using molecular weight standards and fractions were analyzed by Western for the TAP tag. (*C*) Plots of the Western analyses from *B* and other SEC runs. (*D*) Using whole-cell extracts from yeast strains expressing TAP-Set1 and Bre2-Myc (lanes *1*, *3*–*6*) or just TAP-Set1 (lanes *2*, *7*), TAP-Set1 was affinity purified with associated proteins (lanes *3*–*7*). The three *sdc1* mutations were present in lane *4* (*Δsdc1*), lane *5* ($sdc1^{\Delta 121-165}$), and lane *6* (*sdc1**), and lanes *1* and *2* show input without affinity purification. The Western blot was coprobed with anti-TAP and anti-Myc antibodies. (*E*) Expression levels of TAP-Set1 protein in wild-type and *sdc1* mutant strains evaluated by Westerns using whole-cell extracts and β-actin (B-actin) as loading control. (*F*) A second copy of the Set1 gene from −497 to +1179 including an N-terminal Myc-tag was integrated into the TAP-Set1 strain at the *ura3* locus (lanes *1*, *3*, *4*). Total cell extract (input) and immunoprecipitates as indicated were analyzed by Western to detect the Myc (*top* panel) or TAP (*bottom* panel) tags. Lane *2* – TAP-Set1 only. (*G*) Photon counting histogram (PCH) analysis of Set1C in whole-cell extracts from wild-type and *sdc1* mutant strains were compared with strains expressing 1x yEGFP, 2x yEGFP (tandem yEGFP-yEGFP) and 3x yEGFP (tandem yEGFP-yEGFP-yEGFP; Supplemental Fig. S2). Error bars show mean ± SEM from three independent experiments.

per emitting molecule and the number of emitting molecules within the focal volume (Chen et al. 2003). Yeast strains were constructed to express yEGFP as a monomer or tandem dimer or trimer from the same locus (Supplemental Fig. S2), which were then used to establish standard values. A yeast strain expressing yEGFP-Swd1 corresponded to the yEGFP dimer, whereas the same strain with an *sdc1* mutation corresponded to monomeric yEGFP (Fig. 1G).

Taken together with the 386-kDa molecular weight of monomeric Set1C (based on one molecule each of the eight subunits) and the evidence that Sdc1/Dpy30 includes a dimer interface (Wang et al. 2009; Tremblay et al. 2014; Zhang et al. 2015a), these data establish that the ~1MDa Set1C is essentially dimeric, Sdc1 presents the dimer interface, and the three mutant Sdc1 Set1Cs are monomeric.

The distribution of H3K4 methylation by monomeric Set1C is skewed

To explore the functional implications of Set1C dimerism, we compared global H3K4 methylation conveyed by dimeric and monomeric Set1Cs by Western. All three *sdc1* mutations dramatically reduced global trimethylation (H3K4me3), strongly reduced dimethylation (H3K4me2), and moderately reduced monomethylation (H3K4me1) compared with wild type (Fig. 2).

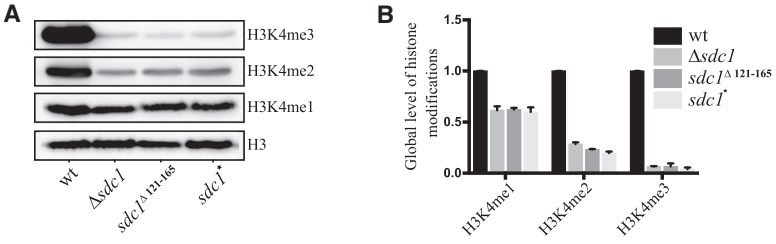

Figure 2. Monomeric Set1C affects global levels of H3K4 methylation. (*A*) Western blot showing global levels of H3 and H3K4me1, H3K4me2 and H3K4me3 in wild-type and *sdc1* mutant strains. (*B*) Quantification of the signals in *A* and two independent repeats. Error bars show mean ± SEM from three independent experiments.

Next, chromatin immunoprecipitation (ChIP) followed by massively parallel DNA sequencing (ChIP-seq) was used to compare the genomic distribution of H3K4me3, 2, and 1 deposited by wild-type dimeric or mutant monomeric Set1Cs. As can be seen in screen shots (Fig. 3A; Supplemental Fig. S3A), all three *sdc1* mutations provoked dramatic and virtually identical alterations in the genomic distribution of H3K4 methylation. Notably, the >10-fold global reduction in H3K4me3 was not distributed evenly. Only a few promoters displayed H3K4me3 peaks and all of the rest had almost no H3K4me3 at all. However, these screen shots appear to show that H3K4me3 peaks in the mutant strains are elevated, whereas the global analysis (Fig. 2) indicates that they should be reduced. Because the H3K4m3 epitope was strongly reduced in the mutant strains, the immunoprecipitation efficiencies from wild-type and mutant chromatin, using the same antibody and genome inputs, will be very different since the ratios of antibody to H3K4me epitope are very different. To address this variance and determine adjustment factors, we repeated the ChIPs with a spike-in input control using wild-type *Schizosaccharomyces pombe* chromatin. Adjusting to the input control indicated that the H3K4me3 peaks in the *sdc1* mutants should be reduced about ninefold (Supplemental Fig. S4), thereby indicating that the H3K4me3 peaks in the monomeric Set1C strains were actually strongly reduced compared with their wild-type counterparts. Similarly, H3K4me2 peaks should be reduced about threefold. These adjustment factors were used to adjust the screen shot peaks to give a comparison with the wild-type peaks (Fig. 3A). For the rest of this study, we used our standard ChIP conditions and unadjusted data because this approach magnified the detectable impact of the mutations, allowing the changes to be more readily observed.

We first discuss alterations of H3K4me3. The >10-fold global reduction in H3K4me3 was not distributed evenly with only about 7% of all promoters (401 of ~5500) displaying detectable H3K4me3 peaks and all of the rest with almost no H3K4me3 at all. K-means clustering organized the *sdc1* mutations into three clusters with the 401 promoters that displayed H3K4me3 peaks conveyed by monomeric Set1C clustered at the top (cluster 1) and the promoters totally lacking H3K4me3 at the bottom (cluster 3; Fig. 3B). As repeatedly noted in many eukaryotes, the size of the H3K4me3 promoter peak correlates closely with the amount of mRNA production from that promoter (Howe et al. 2017; Soares et al. 2017). Despite the K means clustering based on the *Δsdc1* data, this relationship was approximately retained in the intensity plot of Figure 3B, which shows that the size of the wild-type H3K4me3 peak near the TSS (Fig. 3B, wt column) approximately correlated with mRNA production from most to least (Fig. 3B, far right column).

The distribution of H3K4me2 by monomeric Set1C also related to promoter activity. Normally, H3K4me2 is lacking from very active promoters (Fig. 3C, cluster A, wt column; Soares et al. 2017). However, strongly elevated levels were found at very active promoters in the *sdc1* mutations. Again, we used K means clustering to sort the promoters in the mutant *sdc1* strains into three categories according to strongly elevated H3K4me2 (Fig. 3C, top, cluster A), total absence of H3K4me2 (Fig. 3C, bottom, cluster C), and the rest (cluster B), which again approximately correlated with mRNA expression levels (Fig. 3C, far right column). Remarkably, the 401 promoters that displayed H3K4me3 peaks (Fig. 3B, cluster 1) are entirely a subset of the 878 promoters showing strongly elevated H3K4me2 (Fig. 3C, cluster A; Supplemental Fig. S5A). In other words, all 401 promoters with H3K4me3 peaks also displayed H3K4me2.

The distribution of H3K4me1 was also distorted by the *sdc1* mutations (Fig. 3D; Supplemental Fig. S3C); however, the relationship to mRNA expression level was less obvious. Normally, H3K4me1 is lacking from all active promoters; however, more than half of all promoters in the *sdc1* mutant strains displayed some H3K4me1, which we divided into two categories according to bidirectional (top, cluster X) or unidirectional promoters (middle, cluster Y) or no H3K4me1 (cluster Z).

Notably, no differences in H3K4 methylation conveyed by monomeric Set1C with or without Bre2 (i.e., *Δsdc1* or $sdc1^{\Delta 121-165}$ compared with point-mutated $sdc1^{*}$) were observed. This may indicate that Bre2 is not required for H3K4 methylation. However, Bre2 may still contribute in vivo in the absence of Sdc1 through a loose association that was lost upon our biochemical fractionation. Relevant to this possibility, the human homolog of Bre2, ASH2L, not only interacts with DPY30 but also with the human homolog of Swd1, RbBP5 (Avdic et al. 2011; Zhang et al. 2015b), and the equivalent interaction between Swd1 and Bre2 was also observed in the recent Set1C structures (Hsu et al. 2018; Qu et al. 2018).

Shifted H3K4me2 and H3K4me1 deposition by monomeric Set1C

The H3K4me ChIP-seq data were used to generate metagene profiles (Fig. 3E–G). For the 401 genes that displayed H3K4me3 peaks, the H3K4me3 distribution was essentially the same as wild type with the peak on the first transcribed nucleosome and diminishing distribution along the transcribed regions. However, global H3K4me1 and H3K4me2 profiles were strongly shifted toward the TSS, suggesting that the absence of H3K4me3 allowed H3K4me1 and H3K4me2 to occupy normally excluded positions.

Correlation to transcription rate and the oxidative phase of the yeast metabolic cycle

To examine the relationship between the 401 H3K4me3 cluster 1 genes and transcription more closely, we used the mRNA expression levels and transcription rate estimates made by Pelechano et al. (2010) to find that two-thirds (265 of 401; 66%) are among the 1000 most highly expressed genes (Supplemental Table S1). Plotting the relationship between the most highly expressed genes and the 401 H3K4me3 cluster 1 genes using bins of 180 from

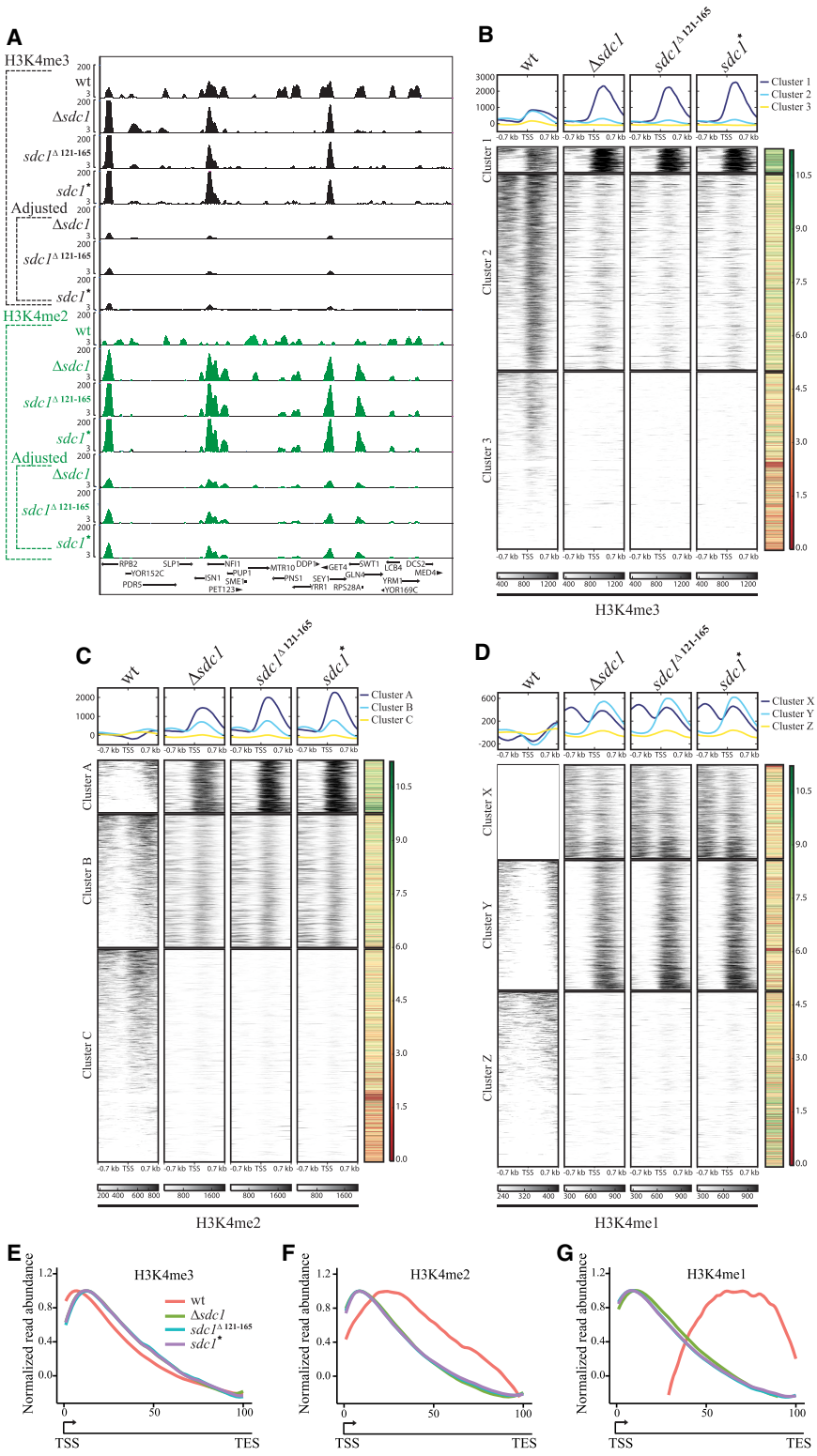

Figure 3. Altered distribution of H3K4 methylation by monomeric Set1C. ChIP-seq results were obtained from two biological repeats for each condition. (*A*) Screen shot of H3K4me3 (*top* half, black) and H3K4me2 (*bottom* half, green) ChIP-seq from wt, *Δsdc1*, *sdc1*$^{\Delta 121–165}$, and *sdc1** strains as indicated with gene diagrams *below*. The raw data from the mutant strains (black and green rows 2–4) were adjusted using the spike-in values (Supplemental Fig. S3) to present adjusted profiles (black and green rows 5–7) for a comparison with wild-type (black and green, rows 1). (*B*) Intensity plots showing H3K4me3 ChIP-seq plotted across a 1.5-kb window centered on TSSs using unadjusted ChIP-seq data. K-means clustering generated three clusters (strong, intermediate, weak H3K4me3 intensity) using the *Δsdc1* data, and then the promoters were stacked according to the strength of the wt H3K4me3 peak downstream from the TSS within each cluster (*left* column; wt). Levels of mRNA expression are shown in the *right*-hand column (color code at the *right*; green, high; red, low). At the *top* of each column, the average profile for each of the three clusters is presented—cluster 1, dark blue; cluster 2, light blue; cluster 3, yellow. (*C*) As for *B*, except plotting H3K4me2 ChIP-seq. K means clustering and then H3K4me2 stacking according to the peak intensities from *Δsdc1* again generated three clusters. These three clusters were independently generated using the H3K4me2 data. Remarkably, the 401 TSSs in cluster 1 of *B* (H3K4me3 peaks) are a subset of the 878 TSSs in cluster A of *C* (H3K4me2 peaks). (*D*) As for *B*, except K means clustering of H3K4me1 ChIP-seq with division into three clusters according to bidirectional promoter regions (cluster X), unidirectional promoter regions (cluster Y), and virtually no H3K4me1 signal (cluster Z). These three clusters do not correspond to the clusters in *B* and *C*. (*E*) Metagene profiles of H3K4me3 peaks from wt (red) and *sdc1* mutant yeast strains. The analysis permuted all gene lengths from TSS to polyadenylation signal (PA) into a scale from 0 to 100. Peak heights were normalized to 1.0. (*F*) As in *A* except for H3K4me2. (*G*) As in *A* except for H3K4me1.

highest to lowest transcription rate displays this clear relationship (Fig. 4A). The same analysis for the 878 H3K4me2 cluster A genes also displays a strong relationship to the transcription rate (Fig. 4A).

In wild-type yeast, Set1C associates with elongating RNA polymerase II, so we evaluated whether monomeric Set1C interaction with Pol II had been altered. However, no change was observed. As previously reported for wild-

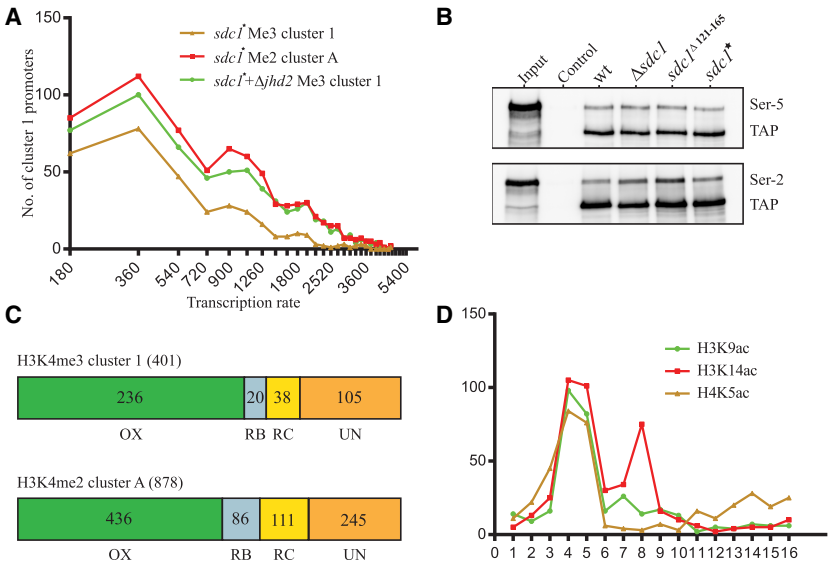

Figure 4. Functional revelations associated with monomeric Set1C. (*A*) The relationship between the 401 promoters with H3K4me3 peaks (brown) or the 878 that acquired H3K4me2 peaks (red) in the monomeric Set1C strain was plotted against transcription rates as described by Pelechano et al. (2010) in bins of 180 genes from highest to lower transcription rate. Also included in this plot is the same analysis for the 787 promoters identified as increased H3K4me3 peaks upon deletion of *jhd2* (green; see Fig. 6). Data is available in Supplemental Table S1. (*B*) TAP-Set1 was immunoprecipitated from whole-cell extracts of wild type and the indicated *sdc1* strains, and evaluated by Westerns using antibodies against phosphorylated Ser5 (*top* panel) or Ser2 (*bottom* panel) of the Pol II CTD tail together with PAP to visualize the TAP tag, as indicated. Control: IgG sepharose was replaced by sepharose in the immunoprecipitation step. (*C*) The 401 H3K4me3 and 878 H3K4me2 promoter peaks were assigned to phases of the yeast metabolic cycle (YMC) using the analysis of Kuang et al. (2014). OX, oxidative; RB, reductive building; RC, reductive charging phases of YMC. UN: Genes unassigned in the YMC data. See also Supplemental Figure S5C,D. (*D*) The 401 H3K4me3 promoters were compared with the YMC H3K9ac, H3K14ac, and H4K5ac ChIP-seq data of Kuang et al. (2014). The plot shows the number of 401 promoters that occur in the top 500 promoters displaying the nominated acetylation in each of the 16 ChIP-seq samples that were taken across the YMC. Samples *3*, *4*, and *5* are in the oxidative phase.

type Set1C (Dehé et al. 2006), immunoprecipitation of TAP-tagged wild type and monomeric Set1 retrieved both Ser5 and Ser2 phosphorylated forms of Pol II (Fig. 4B).

GO term analysis of the 401 genes revealed highly statistically significant relationships especially relating to ribosome biogenesis (Supplemental Fig. S5B), which is not surprising because the genes involved in ribosome biogenesis are among the most highly expressed in yeast. Ribosome biogenesis is also the major feature of the oxidative phase of the yeast metabolic cycle (YMC) (Tu et al. 2005). Therefore, we checked the relationship of the 401 cluster 1 genes to a high-resolution analysis of the YMC (Kuang et al. 2014). A strong correlation to genes in the oxidative (OX) phase emerged (Fig. 4C; Supplemental Fig. S5C) even though OX is the shortest phase occupying one-fifth of the YMC and the other two phases, reductive building (RB) and reductive charging (RC), together occupy four-fifths. Nearly 60% of the 401 genes (236 out of 401) are OX genes with 72 out of 236 distinct from the 265 in the top 1000 highly transcribed genes noted above. Furthermore, a strong correlation between the 401 genes and promoters displaying the three histone acetylation marks that peak in the oxidative phase (H3K9ac, H3K14ac, H4K5ac) (Kuang et al. 2014) was also observed (Fig. 4D). The relationship of the 878 H3K4me2 cluster A genes to the oxidative phase is also strong (Fig. 4C; Supplemental Fig. S5E).

Alterations of gene expression and H3K4 methylation do not correlate

Total mRNA profiles were documented to evaluate the impact of monomerizing Set1C on gene expression. Because complete removal of H3K4 methylation has only a modest effect on gene expression in yeast (Margaritis et al. 2012; Ramakrishnan et al. 2016; Howe et al. 2017), we were not surprised to find that these dramatic alterations in the distribution and levels of H3K4 methylation also had modest effects on gene expression (Supplemental Fig. S6). Overall, only about 4% (211) of all mRNAs were commonly affected more than twofold in all three *sdc1* mutants (Supplemental Fig. S6C,D), and these alterations were evenly spread across expression levels and all three H3K4me3 clusters (Supplemental Fig. S6G–I), so did not correlate with promoter activity. Notably, the 134 commonly affected genes whose expression increased in the three *sdc1* mutant strains were enriched for ribosomal biogenesis (Supplemental Fig. S6F), which is reminiscent of the apparent role of Set1 as a repressor of ribosomal genes (Ramakrishnan et al. 2016). Most of these 134 genes (105 of 134 = 78%) are not in the 401 genes of H3K4me3 cluster 1 or the 878 genes of H3K4me2 cluster A (79 of 134 = 59%), again indicating that alterations of H3K4 methylation and expression did not correlate.

Demethylation by Jhd2 in normal growth is modest

The altered patterns of H3K4 methylation in the monomeric Set1C strains could also be affected by demethylation mediated by the sole yeast Jumonji domain H3K4 demethylase, Jhd2 (Liang et al. 2007; Huang et al. 2010). Before we could address this issue, we first needed to address the controversy surrounding the demethylation activity of Jhd2 in wild-type yeast. Initially, loss of H3K4me3 was reported to be passive through dilution by replication (Ng et al. 2003). Subsequently, a much higher rate of quantitative, Jhd2-dependent, H3K4me3 removal within one cell cycle was reported using a Set1

temperature-sensitive degron (Seward et al. 2007). A more detailed analysis identified both active and passive contributions to demethylation (Radman-Livaja et al. 2010).

To determine whether Jhd2 rapidly demethylates H3K4me3 under normal laboratory growth, we used the auxin inducible degron (AID) (Nishimura et al. 2009) by adding it onto the N terminus of Set1. As performed with the temperature-sensitive degron (Seward et al. 2007), yeast cultures were treated with α-factor to synchronize and reduce cycling before degron activation by indole acetic acid (IAA) administration. AID-Set1 was rapidly degraded upon IAA addition, accompanied by modest reductions of H3K4me2 and H3K4me3 levels, which were partly attributable to Jhd2 (Fig. 5A,B). Notably, the rate of H3K4me3 loss after auxin degron removal of Set1 was much less than that reported using a temperature-sensitive degron (Seward et al. 2007). Because the activity of chromatin regulators is often amplified by stress (Weiner et al. 2012), we considered the possibility that the heat shock used for the Set1 temperature-sensitive degron was the source of the discrepancy. Hence, the auxin degron experiment was repeated to include a shift to 37°C at the time of IAA administration, which revealed rapid H3K4me3 demethylation, some of which was mediated by Jhd2 (Fig. 5C,D). Because temperature shift to 37°C releases yeast from α-factor blockade (Day et al. 2004), passive dilution through histone replacement by cycling could have also contributed to the loss of H3K4me3 in this experiment, as well as other potential mechanisms such as tail cleavage (Duncan et al. 2008; Santos-Rosa et al. 2009). We conclude that H3K4me3 and H3K4me2 demethylation is modest under normal culture conditions and is promoted by heat shock through Jhd2 and another active mechanism.

Jhd2 removes H3K4me3 from many sites of monomeric Set1C deposition

Consistent with this conclusion, deletion of *jhd2* in wild-type yeast under normal growth conditions had only slight effects on total H3K4 methylation (Fig. 5E,F), gene expression (Supplemental Figs. S6A,B, S7), or the distribution of H3K4 methylation (Fig. 6A–C, *Δjhd2* columns; Supplemental Fig. S8). In contrast to these subtle effects, loss of Jhd2 had a pronounced impact on H3K4me3 in the monomeric Set1C yeast strain, which was elevated on most of the 401 cluster 1 promoters (394 of 401) and a further 393

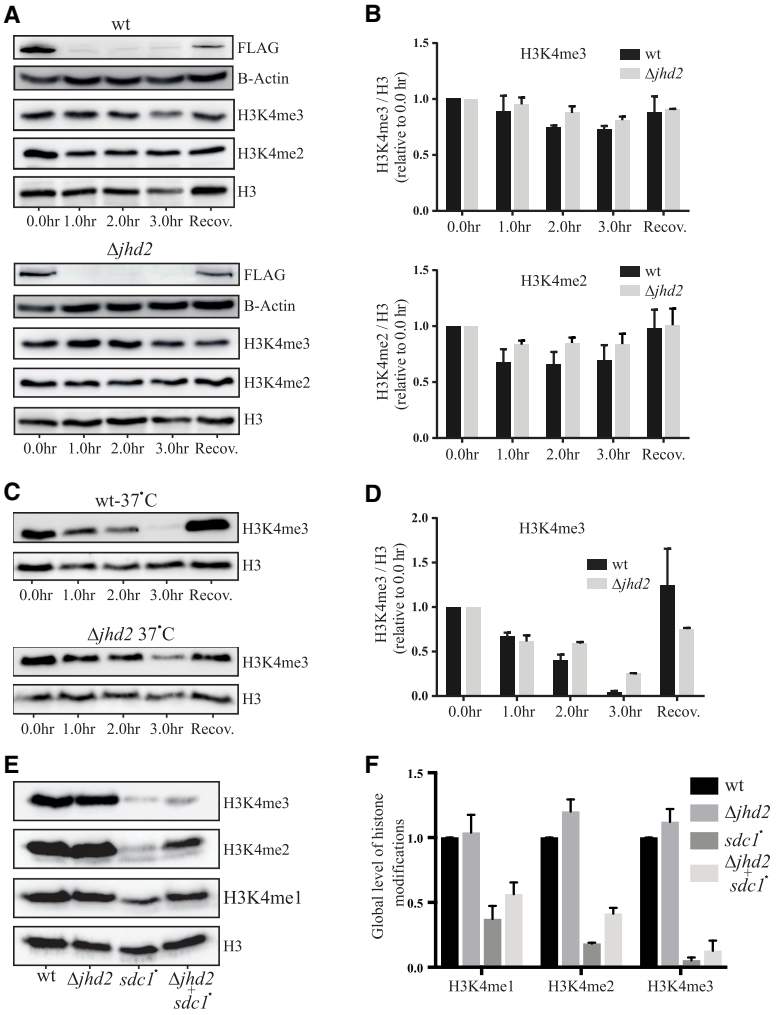

Figure 5. Demethylation by Jhd2. (*A*) Time courses after IAA administration in a strain expressing OsTir1 with AID-Set1 (*top* panel) and AID-Set1/*Δjhd2* (*bottom* panel). Western analyses were performed with antibodies against the epitopes indicated at the *right*. Recovery (Recov.) was harvested 2 h after IAA washout. (*B*) Quantification of H3K4me3 (*top* histogram) and H3K4me2 (*bottom* histogram) of the experiment in *A* and two repeats, normalized to H3 levels. Error bars; mean ± SEM from three independent experiments. (*C*) The same experiment as *A* performed at 37°C. (*D*) Quantification of H3K4me3 from the experiment in *C* as described in *B*. (*E*) Western blot showing global levels of H3 and H3K4me1, H3K4me2, and H3K4me3 in wt, *Δjhd2*, *sdc1**, and *sdc1** + *Δjhd2* strains. (*F*) Quantification of the signals in *E* and two repeats. Error bars, mean ± SEM.

cluster 2 promoters previously lacking H3K4me3 peaks (Fig. 6A,D). This reveals that a substantial amount of H3K4me3 deposited by monomeric Set1C is removed by Jhd2. In contrast, loss of Jhd2 resulted in only slight alterations of the H3K4me1 and H3K4me2 patterns (Fig. 6B, C). The spike-in control (Supplemental Fig. S4) indicated an adjustment factor of fourfold, which was used in Figure 6D to again provide a visual comparison to wild type.

The 787 (394 + 393) increased H3K4me3 peaks strongly overlap with the previously defined categories with 87% (684 of 787) also H3K4me2 cluster A genes (Supplemental Fig. S5A). The 787 increased H3K4me3 peaks also strongly related to the transcription rate (Fig. 4A) and the YMC OX genes (Supplemental Fig. S5E).

We used transcriptome profiling to evaluate the impact of *jhd2* deletion in combination with the *sdc1* point mutation. Deletion of *jhd2* had no effect on wild-type gene expression and a modest impact when combined with point mutated *sdc1* (Supplemental Fig. S7). Despite robust data quality (Supplemental Fig. S6A,B), of the 558 mRNAs that were altered more than twofold in the point mutated *sdc1* strain, 327 (59%) were similarly altered in the double mutant strain (Supplemental Fig. S7A,B). Again, these gene expression changes were evenly distributed regardless of expression levels or promoter activity from strong to weak (Supplemental Fig. S7E–G) and consequently did not correlate with H3K4me3 alterations.

Monomeric Set1C produced increased levels of asymmetric H3K4me nucleosomes

As recently evaluated (Soares et al. 2017) and also observable in Figure 3B–D, H3K4me2 and H3K4me1 are excluded from the H3K4me3 nucleosomes that surround promoters in wild-type yeast and the degree of exclusion relates to the transcriptional activity of the promoter. For highly expressed genes, both H3K4me2 and H3K4me1 are completely excluded. For moderately expressed genes, H3K4me1 but not H3K4me2 is excluded. For lowly expressed genes, both H3K4me1 and H3K4me2 infiltrate promoter nucleosomes (Fig. 3B–D, wt panels). Monomeric Set1C changed these patterns with H3K4me3 reduced on all promoters, whereas H3K4me1 and H3K4me2 are increased on active promoters (Figs. 3B–G, 6A–C; Supplemental Fig. S8). To evaluate whether this represents a shift from symmetrical H3K4me3 nucleosomes to asymmetrical H3K4me3 combined with H3K4me1 or H3K4me2, we scaled up the ChIP procedure fourfold using mononucleosomes (Supplemental Fig. S9) and analyzed the H3K4me3 immunoprecipitates by Western for H3K4 methylation. This analysis clearly revealed elevated levels of asymmetrically H3K4me modified nucleosomes in the monomeric Set1C strains (Fig. 6E,F).

Discussion

Until recently, the inherent symmetry of the nucleosome promoted the assumption that posttranslational modifications would also be symmetrical. The identification of asymmetrically modified nucleosomes at promoters (Voigt et al. 2012; Rhee et al. 2014) revealed a new level of epigenetic detailing, which could convey greater combinatorial specificities and/or impose directional orientation in chromatin. One hit stochastic deposition was the first proposition for the origin of nucleosomal posttranslational asymmetry (van Rossum et al. 2012). Our finding that Set1C is dimeric introduces the new perception that the deposition of a posttranslational modification is inherently symmetrical because the responsible enzyme is also symmetrical. This proposition has several implications that we first discuss in light of the recent high-resolution structures of the Set1C enzymatic core (Hsu et al. 2018; Qu et al. 2018).

Both the recent crystal and cryo-EM structures present the core of the Set1C/COMPASS complex as monomeric centered on the C terminus of Set1 with the Swd3/Swd1 heterodimer (Roguev et al. 2001) on one side and the Bre2/Sdc1 heteromer (Roguev et al. 2001) on the other. In both structures, all five components are monomeric except Sdc1, which is a dimer based on the RIIa dimer interface. One Sdc1 interacts with Bre2 through its' Bre2 interaction site (South et al. 2010) and the Bre2 interaction site of the other Sdc1 is exposed (Hsu et al. 2018). Consequently, dimeric Set1C can be readily accommodated with these high-resolution structures by replacing the exposed Sdc1 with the mirror image of the Sdc1/Bre2 interaction (Fig. 7A) to infer a V-shaped structure of the dimeric Set1C complex (Fig. 7B). From differences between two cryo-EM structures, Qu et al. (2018) speculated that flexible curvature of the monomeric structure could present a binding site to accommodate a nucleosome. We extend this idea to suggest that (1) this flexible curvature is reciprocated in dimeric Set1C to bind a nucleosome symmetrically (Supplemental Fig. S10) and (2) the study of Set1C nucleosomal binding needs to be performed with the dimeric complex.

It is not clear why both crystal and cryo-EM Set1C structures are not dimeric. Both structural studies utilized baculoviral coexpression of truncated versions of Set1 with full-length Swd1, Swd3, Bre2, and Sdc1. Possibly co-overexpression in fly cells or some other associated methodological practice disfavored the acquisition of the dimeric complex. Alternatively, the lack of dimerism may be due to the parts of Set1C that were omitted from baculoviral overexpression, including most of Set1 itself and two subunits, Swd2 and Shg1. In addressing this conundrum, we also considered the possibility that Set1C may transition between monomeric and dimeric versions. Yeast Set1C was estimated at 800–1000 kDa by three different studies (Miller et al. 2001; Roguev et al. 2003; Trésaugues et al. 2006). However, a fourth study reported a 500-kDa size (Nagy et al. 2002). These different size estimations correlate with different growth conditions. The three 800–1000 kDa estimations were obtained from exponential growth, whereas the 500-kDa estimation was obtained from yeast grown to saturation in a large fermenter. To examine the correlation, we estimated Set1C size from saturated yeast cultures and observed a proportion of a smaller complex (Supplemental Fig. S10).

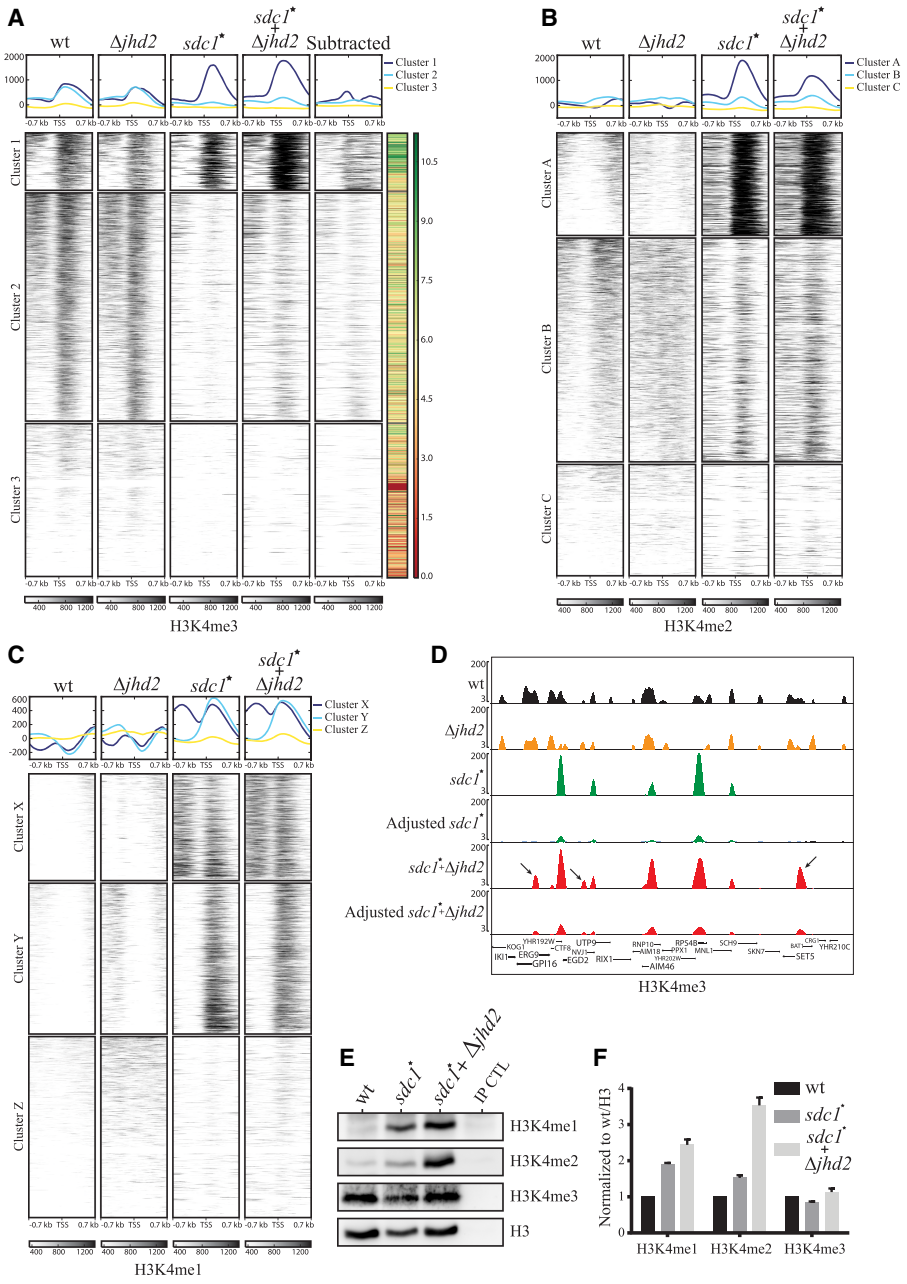

Figure 6. Jhd2 demethylation of asymmetric H3K4me3 deposited by monomeric Set1C. (*A*) As for Figure 3B, intensity plots display ChIP-seq enrichment for H3K4me3 plotted across a 1.5-kb window centered on TSSs. The three clusters identified by K means clustering are the same as Figure 3B. The "subtracted" column is the result of subtracting column *sdc1** from column *sdc1** + *Δjhd2* to illustrate the effect of Jhd2 demethylation. mRNA expression levels are shown in the *right*-hand column (color code at the *right*). (*B*) As for *A*, intensity plots showing ChIP-seq enrichment for H3K4me2 plotted across a 1.5-Kb window centered on TSSs. The three clusters identified by K means clustering are the same as for Figure 3C. (*C*) As for *A*, intensity plots showing ChIP-seq enrichment for H3K4me1 plotted across a 1.5-kb window centered on TSSs. The three clusters are the same as Figure 3D. (*D*) Screen shot of H3K4me3 profiles from the indicated strains. Arrows indicate some peaks that appear when *jhd2* was mutated in the *sdc1** strain. *Beneath* the raw *sdc1** (green) and *sdc1** + *Δjhd2* (red) profiles are adjusted profiles using the spike-in the adjustment factors calculated in Supplemental Figure S3. (*E*) H3K4me3 mononucleosomes were immunoprecipitated from wt, *sdc1**, and *sdc1** + *Δjhd2* strains and analyzed for H3K4me1, H3K4me2, and H3K4me3 normalized to H3 by Western. The H3K4me3 antibody was omitted from the immunoprecipitation control (IP CTL). Supplemental Figure S9 shows full gel images. (*F*) Quantitation using densitometry of the Western bands of the experiment in *E* and two biological repeats.

Whether the smaller complex is physiologically relevant and why the overexpressed baculoviral core Set1Cs are monomeric are questions that require further work to answer. However, Hsu et al. (2018) noted that the intrinsic instability of Bre2 is stabilized by Sdc1. Although this stabilization does not require Sdc1 dimerization (Fig. 1D), possibly the Bre2–Sdc1 interaction is an inherently weak aspect of dimeric Set1C.

Mutagenesis of the Set1C dimer interface enabled a ChIP-seq comparison of the genomic H3K4 methylation

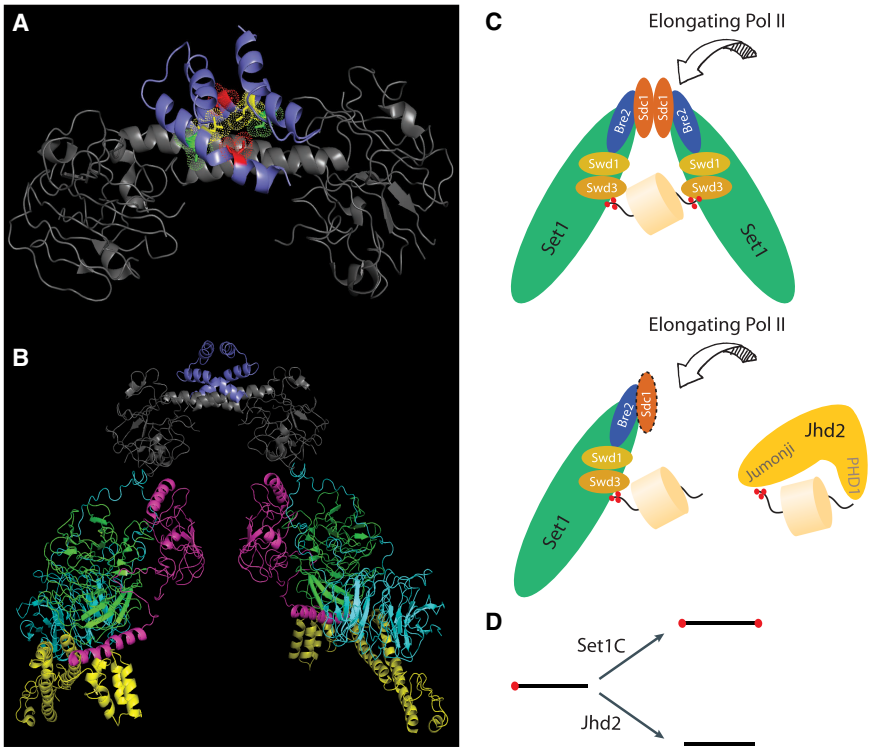

Figure 7. Models for action by Set1C and Jhd2. (*A*) The Set1C dimer interface extrapolated from the cryo-EM structure of Qu et al. (2018) by duplicating the Sdc1 (blue) bound to Bre2 (gray) as a mirror image. The three residues V129, L133, and L134 mutated to alanines to disrupt Sdc1 dimerization are depicted in yellow, green, and red. (*B*) The core of Set1C represented as a dimer based on a mirror image of the cryo-EM structure of Qu et al. (2018) as in *A* excluding the colored alanine mutations and including the rest of the core Set1C with the SET domain (magenta), Swd 1 (light blue), Swd 3 (green), and Spp1 (yellow). (*C*) Wild-type, dimeric, Set1C is introduced by elongating Pol II to symmetrically trimethylate promoter nucleosomes at H3K4. Other factors and cues modulate this process. The Sdc1 dimer interface associates with Set1C through interaction with Bre2. The other WRAD heteromer, Swd1/Swd3, is required for methylation (Wdr5 = Swd1, Rbbp5 = Swd3, Ash2l = Bre2, and Dpy30 = Sdc1). When Sdc1 is mutated, Set1C is monomeric. It is still introduced by elongating Pol II to promoter nucleosomes to trimethylate H3K4, but only on one tail, leaving asymmetrically modified nucleosomes. Asymmetric H3K4me3 nucleosomes are detrimethylated by Jhd2 through recognition of the un/monomethylated tail by its' PHD1 finger. (*D*) Dimeric Set1C and monomeric Jhd2 act in concert to reduce asymmetrical H3K4me3.

distribution in wild-type dimer and mutant monomeric Set1C yeast strains. Importantly, mutagenesis of the dimer interface did not interfere with the association of Set1C with elongating RNA Pol II. Based on this association and the widespread correlation between mRNA levels and the size of H3K4me3 promoter peaks, it is widely presumed that H3K4me3 deposition on promoter nucleosomes follows transcription of the associated gene (Howe et al. 2017; Woo et al. 2017) and the high-resolution YMC analysis (Kuang et al. 2014) supports this notion. Whereas H3K4me3 peaks in wild-type yeast smoothly relate to the amount of mRNA produced, only 401 promoters displayed detectable H3K4me3 peaks in the monomeric Set1C strains. Furthermore, in the monomeric Set1C yeast strains, both H3K4me2 and H3K4me1 infiltrated active promoters from which they are normally excluded and the 401 H3K4me3 promoters are a subset of the 878 promoters that showed strong H3K4me2. Both the 401 and 878 genes are strongly related to high transcription rates and the YMC oxidative phase.

Removal of the sole yeast H3K4 demethylase, Jhd2, provided insight. Whereas Jhd2 removal in a wild-type background had virtually no effect on H3K4 methylation patterns or gene expression, Jhd2 removal from a monomeric Set1C strain resulted in increased H3K4me3 both on the 401 cluster 1 promoters (394 of 401) and also on another 393 promoters, which, together, were largely (787 of 878 = 90%) the same as the 878 H3K4me2 cluster A promoters. Therefore, certain mechanisms directed the monomeric Set1C to a subset of active promoters that acquired H3K4me2, some of which also present H3K4me3 and most of which were also demethylated by Jhd2 from H3K4me3 to H3K4me2. These mechanisms correlate with high transcriptional activity and the YMC oxidative phase, possibly through recognition of acetylations at H3K9, H3K14, and/or H4K5. However, none of these correlations appear to be comprehensive. Potentially another factor or combination of factors is required to fully account for the promoter selectivity of monomeric Set1C.

Normally, H3K4me3 deposited by dimeric Set1C is not removed by Jhd2, whereas a substantial fraction of H3K4me3 deposited by monomeric Set1C was removed by Jhd2. Therefore, H3K4me3 deposited by monomeric and dimeric Set1Cs differ in some respect. Immunoprecipitation of H3K4me3 mononucleosomes indicated that increased H3K4me asymmetry is the notable difference.

Jhd2 is expressed as a monomer without associated proteins (Liang et al. 2007). Furthermore, recent in vitro evidence using KDM5A, one of the human homologs of Jhd2, revealed that PHD1 zinc finger, which is highly conserved in Kdm5 demethylases including Jhd2, binds to the H3 tail with the preference H3K4me0 > me1 > me2 > me3, and when bound, stimulates H3K4me3 demethylation by the Jhd2 Jumonji domain (Torres et al. 2015). Evidence from KDM5B also supports a key role for PHD1 in binding H3K4me0 and demethylation (Klein et al. 2014; Zhang et al. 2014). We extend these observations to suggest that stimulation is exerted when PHD1 binds one H3 tail on asymmetrical H3K4me3 nucleosomes (Fig. 7C).

The combination of symmetrical H3K4 trimethylation conveyed by dimeric Set1C with asymmetric H3K4me3 demethylation conveyed by monomeric Jhd2 provokes a remarkable conclusion. Rather than methylation and demethylation acting in opposition as logic would suggest, the two processes act in concert to reduce asymmetric H3K4me3 and thereby focus symmetry onto selected nucleosomes (Fig. 7D). A juxtaposition of concerted addition and singleton removal could also apply to create symmetry and organization on other symmetrical substrates and circumstances.

This concept also provides some clarity regarding the action of Kdm5/Jarid 1 class of demethylases, which may have relevance for other classes of histone demethylases. As reported by others (Tu et al. 2007; Ramakrishnan et al. 2016) and again documented here, loss of Jhd2 has almost no effect in yeast grown under normal laboratory conditions. Also, mouse knockout phenotypes of the Kdm5/Jarid1 genes have been difficult to interpret because they present incompletely penetrant phenotypes (Schmitz et al. 2011; Scandaglia et al. 2017). Concordant with studies on Kdm5b in embryonic stem cells (Kidder et al. 2014), we suggest that an ancillary editing role in the epigenetic definition of chromatin offers an explanation for the incompletely penetrant phenotypes of these highly conserved enzymes. Under optimal circumstances their contribution is unnecessary, but in certain circumstances the demethylases serve to reduce errors. That is, the Kdm5/Jarid1 demethylases add correctional stability to gene expression programs by focusing H3K4me3 onto promoter nucleosomes.

Similarly, the role of Set1 and H3K4 methylation in yeast has been a source of confusion largely due to its apparent dispensability and the counter-intuitive observation that more genes show increased rather than decreased expression when Set1 is removed (Lenstra et al. 2011; Margaritis et al. 2012). Our observations add more confidence to the presumption that H3K4me3 on promoter nucleosomes is a consequence of the association of Set1C with the elongating polymerase (Howe et al. 2017; Soares et al. 2017; Woo et al. 2017). Given the conserved role of the H3K4me3 epitope as a binding site for protein complexes involved in transcriptional initiation such as TFIID (Vermeulen et al. 2007), a contribution to the stability of gene expression, rather than a role in its regulation, appears to be the most robust explanation.

Along with TFIID and other complexes involved in transcriptional initiation, H3K4me3 is also bound by Set1C itself through the PHD finger in Spp1 (Shi et al. 2007; Eberl et al. 2013). Spp1 binding of H3K4me3 could serve as a feed-forward epigenetic mechanism to propagate H3K4me3 after replication. Alternatively, our new perceptions about H3K4me3 symmetry on promoter nucleosomes suggest that Spp1 could serve in other ways. If delivery of Set1C to the promoter nucleosomes by its association with elongating polymerase resulted in one-hit, stochastic deposition, then Spp1 binding could serve to attach Set1C to the hemi-trimethylated nucleosome for trimethylation of the other tail. Another possibility involves an allosteric role for Spp1 binding within the dimeric complex to enhance the efficiency of symmetrical trimethylation.

We favor the second explanation because the difference between H3K4me3 deposition by monomeric or dimeric Set1Cs suggests that monomeric Set1C deposition is stochastic, whereas dimeric Set1C deposition includes cooperativity to which Spp1 binding to H3K4me3 may contribute. This possibility concords with the cryo-EM structure, which includes Spp1. Although the PHD finger was not resolved, the authors suggest that its proximity may permit a contribution to substrate binding (Qu et al. 2018).

We suggest that in response to transcriptional activity and subsequent verification according to oxidative phase and other unidentified cues, dimeric Set1C symmetrically trimethylates both H3K4 residues on promoter nucleosomes. Deposition by monomeric Set1C also reflects transcriptional activity and the other verification cues; however, it does not engage in dual deposition but rather one-hit action, resulting in asymmetrically trimethylated nucleosomes. When the transcription rate and/or other cues are higher than a certain level, sufficient stochastic deposition by monomeric Set1C achieves symmetrical trimethylation of some promoter nucleosomes, which then resist demethylation by Jhd2 because H3K4me3 is symmetrical (Fig. 7C).

Our observations do not permit conclusions about symmetry regarding H3K4me1 and H3K4me2 deposition. However, if dimeric Set1C binds to a nucleosome and accesses both H3 tails, catalytic symmetry for monomethylation and dimethylation is likely.

The SET domain-WRAD scaffold is among the most highly conserved protein modules in eukaryotic epigenetics and all H3K4 methyltransferase complexes appear to include Dpy30/Sdc1 (Ruthenburg et al. 2007; Rao and Dou 2015). Therefore, it is likely that all Set1/Trithorax-type H3K4 methyltransferase complexes are dimeric and their deposition of methyl groups in chromatin is, like Set1C, also an embedded product of dimerism. This implies that H3K4me3 nucleosomes are implicitly symmetrical for H3K4me3 and asymmetrical H3K4me3 nucleosomes, such as bivalent nucleosomes (Voigt et al. 2012, 2013; Shema et al. 2016), are the product of asymmetric demethylation or interference with the propensity of the bivalent H3K4 methyltransferase, Mll2 (Denissov et al. 2014) to methylate both H3 tails in the same nucleosome.

Using the auxin degron, we observed that bulk H3K4me3 and H3K4me2 turnover in yeast is modest. Attempting to understand previous results (Seward et al. 2007), we found that H3K4me3 loss is promoted by heat shock, which may contribute to the accompanying widespread changes in gene expression. Notably, less than half of the H3K4me3 loss could be attributed to Jhd2 and another mechanism for demethylation is clearly indicated. Under stress such as heat shock, it appears that symmetrical H3K4me3 nucleosomes can be disturbed possibly to generate asymmetrical H3K4me3 nucleosomes that Jhd2 acts upon. Alternatively, heat shock may activate Jhd2. In either case, examination of the impact of stress on demethylation could be fruitful.

Materials and methods

Additional methods are described in the Supplemental Material.

Tagging

Set1 was N-terminally tagged because C-terminal tagging inactivates the methyltransferase activity (Roguev et al. 2001). The AID-Flag cassette was directed between the 2nd and 3rd amino acid codons of the Set1 gene by insertion of KanMx selection gene flanked by loxP sites and selection for G418 resistance. After Cre recombination, a 34-bp loxP site was left in the reading frame between AID-Flag and the rest of the Set1 coding region.

Protein assays and immunoblotting

For SEC, a 10/30 Superose 6 size exclusion column (HR, Pharmacia) was loaded with 500 µL of cleared crude cell extract from a TAP-tagged strain and run in glycerol-free buffer E (20 mM HEPES-NaOH at pH 8.0; 350 mM NaCl; 0.1% Tween 20; 10% glycerol; 1 µg each of leupeptin, aprotinin, and pepstatin A; 1 mM phenylmethylsulfonyl fluoride) (Logie and Peterson 1999). Fractions were resolved on an 8% SDS-polyacrylamide gel and analyzed by immunoblotting with peroxidase–antiperoxidase (PAP) (Sigma) diluted 1:1000, for detection of the protein A region within the TAP tag using the ECL kit (Amersham Pharmacia Biotech).

Antibodies

Antibodies used in this study were as follows: α-Myc antibody (Myc; 9E10; Roche Applied Science, catalog no. 11667203001), PAP antibody (Sigma, catalog no. P1291), H3K4me1 (1:2000; Diagenode, pAB-037-050), H3K4me2 (1:1000; Diagenode, pAB-035-050), H3K4me3 (1:1000; Abcam, ab8580), H3 (1:2000; Abcam, ab1791), CTD Ser2 phosphorylation (1:1000; Abcam, ab5095), and CTD Ser5 phosphorylation (1:1000; Abcam, ab5131).

FCS

Swd1 was C-terminally tagged with yeast codon optimized EGFP. To generate yeast strains expressing yEGFP as a monomer or tandem dimer or trimer, the coding sequence of yEGFP was PCR amplified with a forward primer containing the initiating codon along with a 5′ 40-bp homology arm to the integration vector, YIplac211, and a reverse primer containing HindIII and BamHI sites along with a 3′ 40-bp homology arm. Linearized YIplac211 and the PCR fragment were then recombined by full-length RecE/RecT recombination (Fu et al. 2012). To create the tandem dimer of yEGFP a PCR fragment was amplified with a forward primer carrying a HindIII site with a 9-bp spacer (GCTGGTTTA) along with a reverse primer carrying SpeI, PstI, and BamHI sites. The 1xEGFP vector and the PCR product were digested with HindIII and BamHI, then ligated. To further create the tandem trimeric yEGFP, a PCR fragment was amplified with a forward primer carrying an SpeI site with a spacer sequence as above in combination with a reverse primer carrying a PstI site. The PCR fragment and the tandem 2xyEGFP were digested with SpeI and PstI and ligated. The resulting plasmids were verified by DNA sequencing, linearized, and integrated into the genome (URA3).

For FCS, whole-cell extracts were prepared from 50 OD of exponentially growing cells by bead beating in buffer E. The clarified extracts were measured using Labtek chambers coated with 1 mg/mL BSA for 30 min and washed with PBS twice. In FCS, the changes in fluorescence intensity reflect the fluctuations of the number of particles as a function of time. Samples were diluted so that, on average, five molecules were present in the detection volume at a time. The average number of molecules was calculated for a serial dilution series by fitting the autocorrelation curves with a single component fitting:

$$G(\tau) = \frac{1}{N}\left(1 + \frac{\tau}{\tau D}\right)^{-1}\left(1 + \frac{\tau}{\omega^2 \tau D}\right)^{1/2},$$

where N is the average particle number of species in the sampling volume and τ_D is the residence time of species within the sampling volume, with $\tau_D = \omega^2_{xy}/8D$ with D the diffusion coefficient of the species and $\omega = \omega_z/\omega_{xy}$ the aspect ratio of the sampling volume. For measuring the stoichiometry of Set1C in wild-type and *sdc1* mutants in cell extracts, intensity distributions were obtained using a Zeiss LSM 780 confocal microscope in fluorescence-correlation spectroscopy and photon-counting histogram mode. To quantify molecular brightness, we used fluorescence intensity distribution analysis (FIDA), which discriminates different fluorescent species according to their molecular brightness. FIDA was performed as described (Kask et al. 1999) and the experiment was repeated independently three times.

Auxin-inducible degron

To make strains for the auxin-inducible degradation experiment, pURA3-pAHD1-mTIR1-CYC1-pA carrying the ADH1 promoter to express OsTIR1 was integrated at the URA3 locus to obtain RC125. Then, an N-terminal AID-Flag tag was added to the N terminus of *set1* to obtain RC126. *jhd2* was deleted in this strain to obtain RC127. Overnight cultures were inoculated into fresh YEPD (O.D. 0.1), grown to O.D. 0.4 at the respective temperatures. Cells were then arrested by adding α-factor to 15 nM for 4–6 h. To induce degradation, 3-indoleacetic acid (IAA; Sigma, I2886) was added to a final concentration of 0.5 mM.

ChIP-seq analysis

ChIP-seq reads were mapped to sacCer3 *S. cerevisiae* genome assembly using BWA and parallel version of pBWA (0.5.9-r32-MPI-patch2). After mapping, uniquely mapped reads were filtered (-q 1) and PCR duplicates (reads with same start and mapped to same strand) were removed using Samtools (rmdup) (Li and Durbin 2010). Read lengths were computationally extended to 150-bp strand specifically and stored in Bam format. The Bam files were subject to coverage calculation using the bamCoverage utility of deepTools (Ramírez et al. 2014) for a sliding window of 40 bp, normalized using RPKM parameters, and stored in BigWig format. Additionally, these files were then subtracted by the mock IP control. Thus, all of the resultant data were directly comparable because of RPKM normalization and control subtraction. Several data matrices were created for different loci of TSS ± 1.5KB, averaged metagene from the BigWig files via computeMatrix and visualized using plotHeatmap utilities of deepTools (also referred to as high-resolution intensity plots or heatmaps). GO analysis was performed using the web-based tool FuncAssociate (Berriz et al. 2003). Composite profile plots were generated using custom code in R statistical language where the input was the above computed matrices using deepTools. BigWig files were visualized as coverage tracks using the UCSC genome browser (Karolchik et al. 2008).

For qChIP experiments, reads were first aligned to sacCer3 reference and then to sPombe reference genomes (obtained via PomBase) (McDowall et al. 2015). Note that reads were independently aligned to both genomes, thus allowing for common mappings as compared with leftover read alignment to reduce the mismatch bias. Percentage of reads aligned per sample per genome was documented in a tabular format.

RNA sequencing (RNA-seq) analysis

RNA-seq data were processed mostly using Tuxedo suite and custom scripts for further downstream analysis (Trapnell et al. 2012). Tuxedo suite consists of TopHat (aligns the reads and map them to the genome) (Trapnell et al. 2009), Cufflinks (uses the read alignment map to assemble reads into transcripts) (Trapnell et al. 2010), Cuffdiff (takes aligned reads from multiple conditions and performs differential gene expression analysis) (Trapnell et al. 2013). The counts were calculated and recorded in an expression unit of "fragments per kilobase of exon model per million mapped reads" (RPKM). We used a cutoff of FPKM > 4 for a gene to be called as expressed. Plots were generated using cummeRbund and custom scripts written in R statistical language.

Data availability

The ChIP-seq and RNA-seq data used in this study have been deposited under NCBI BioProject (PRJNA524491).

Acknowledgments

Thanks to Dani Fujimori and Jon Wilson for discussions and Vincent Geli for providing the Myc-tagged version of Set1. Thanks also to the Dresden Genome Center, led by Andreas Dahl, for ChIP-seq and RNA-seq Ilumina sequencing, and Andreas Petzold for initial data handing. This work was supported by funding to A.F.S. from the Deutsche Forschungsgemeinschaft (grant STE 903/7-3) and the European Union 7th framework integrated project Systems Biology of Stem Cells and Reprogramming (SyBoSS).

Author contributions: R.C. performed all the experiments except for the massively parallel DNA sequencing and Figure 1G which was performed with S.A. The computational analyses were performed by S.S. with additional contributions by R.C., A.R., and A.F.S. The project was based on initial results from A.R. The experiments were planned and the manuscript written by R.C. and A.F.S.

References

Avdic V, Zhang P, Lanouette S, Groulx A, Tremblay V, Brunzelle J, Couture JF. 2011. Structural and biochemical insights into MLL1 core complex assembly. *Structure* **19:** 101–108. doi:10.1016/j.str.2010.09.022

Berriz GF, King OD, Bryant B, Sander C, Roth FP. 2003. Characterizing gene sets with FuncAssociate. *Bioinformatics* **19:** 2502–2504. doi:10.1093/bioinformatics/btg363

Bledau AS, Schmidt K, Neumann K, Hill U, Ciotta G, Gupta A, Torres DC, Fu J, Kranz A, Stewart AF, et al. 2014. The H3K4 methyltransferase Setd1a is first required at the epiblast stage, whereas Setd1b becomes essential after gastrulation. *Development* **141:** 1022–1035. doi:10.1242/dev.098152

Catchpole S, Spencer-Dene B, Hall D, Santangelo S, Rosewell I, Guenatri M, Beatson R, Scibetta AG, Burchell JM, Taylor-Papadimitriou J. 2011. PLU-1/JARID1B/KDM5B is required for embryonic survival and contributes to cell proliferation in the mammary gland and in ER+ breast cancer cells. *Int J Oncol* **38:** 1267–1277. doi:10.3892/ijo.2011.956

Chen Y, Wei L-N, Müller JD. 2003. Probing protein oligomerization in living cells with fluorescence fluctuation spectroscopy. *Proc Natl Acad Sci* **100:** 15492–15497. doi:10.1073/pnas.2533045100

Day A, Schneider C, Schneider BL. 2004. Yeast cell synchronization. *Methods Mol Biol* **241:** 55–76. doi:10.1385/1-59259-646-0:55

Dehé P-M, Dichtl B, Schaft D, Roguev A, Pamblanco M, Lebrun R, Rodríguez-Gil A, Mkandawire M, Landsberg K, Shevchenko A, et al. 2006. Protein interactions within the Set1 complex and their roles in the regulation of histone 3 lysine 4 methylation. *J Biol Chem* **281:** 35404–35412. doi:10.1074/jbc.M603099200

Denissov S, Hofemeister H, Marks H, Kranz A, Ciotta G, Singh S, Anastassiadis K, Stunnenberg HG, Stewart AF. 2014. Mll2 is required for H3K4 trimethylation on bivalent promoters in embryonic stem cells, whereas Mll1 is redundant. *Development* **141:** 526–537. doi:10.1242/dev.102681

Dou Y, Milne TA, Tackett AJ, Smith ER, Fukuda A, Wysocka J, Allis CD, Chait BT, Hess JL, Roeder RG. 2005. Physical association and coordinate function of the H3 K4 methyltransferase MLL1 and the H4 K16 acetyltransferase MOF. *Cell* **121:** 873–885. doi:10.1016/j.cell.2005.04.031

Duncan EM, Muratore-Schroeder TL, Cook RG, Garcia BA, Shabanowitz J, Hunt DF, Allis CD. 2008. Cathepsin L proteolytically processes histone H3 during mouse embryonic stem cell differentiation. *Cell* **135:** 284–294. doi:10.1016/j.cell.2008.09.055

Eberl HC, Spruijt CG, Kelstrup CD, Vermeulen M, Mann M. 2013. A map of general and specialized chromatin readers in mouse tissues generated by label-free interaction proteomics. *Mol Cell* **49:** 368–378. doi:10.1016/j.molcel.2012.10.026

Ernst P, Vakoc CR. 2012. WRAD: enabler of the SET1-family of H3K4 methyltransferases. *Brief Funct Genomics* **11:** 217–226. doi:10.1093/bfgp/els017

Ernst P, Fisher JK, Avery W, Wade S, Foy D, Korsmeyer SJ. 2004. Definitive hematopoiesis requires the mixed-lineage leukemia gene. *Dev Cell* **6:** 437–443. doi:10.1016/S1534-5807(04)00061-9

Fu J, Bian X, Hu S, Wang H, Huang F, Seibert PM, Plaza A, Xia L, Müller R, Stewart AF, et al. 2012. Full-length RecE enhances linear–linear homologous recombination and facilitates direct cloning for bioprospecting. *Nat Biotechnol* **30:** 440–446. doi:10.1038/nbt.2183

Glaser S, Lubitz S, Loveland KL, Ohbo K, Robb L, Schwenk F, Seibler J, Roellig D, Kranz A, Anastassiadis K, et al. 2009. The histone 3 lysine 4 methyltransferase, Mll2, is only required briefly in development and spermatogenesis. *Epigenetics Chromatin* **2:** 5. doi:10.1186/1756-8935-2-5

Hödl M, Basler K. 2012. Transcription in the absence of histone H3.2 and H3K4 methylation. *Curr Biol* **22:** 2253–2257. doi:10.1016/j.cub.2012.10.008

Howe FS, Fischl H, Murray SC, Mellor J. 2017. Is H3K4me3 instructive for transcription activation? *Bioessays* **39:** 1–12. doi:10.1002/bies.201670013

Hsu DR, Chuang PT, Meyer BJ. 1995. DPY-30, a nuclear protein essential early in embryogenesis for *Caenorhabditis elegans* dosage compensation. *Development* **121:** 3323–3334.

Hsu PL, Li H, Lau HT, Leonen C, Dhall A, Ong SE, Chatterjee C, Zheng N. 2018. Crystal structure of the COMPASS H3K4 methyltransferase catalytic module. *Cell* **174:** 1106–1116.e9. doi:10.1016/j.cell.2018.06.038

Huang F, Chandrasekharan MB, Chen YC, Bhaskara S, Hiebert SW, Sun ZW. 2010. The JmjN domain of Jhd2 is important for its protein stability, and the plant homeodomain (PHD) finger mediates its chromatin association independent of H3K4 methylation. *J Biol Chem* **285:** 24548–24561. doi:10.1074/jbc.M110.117333

Jiang H, Shukla A, Wang X, Chen WY, Bernstein BE, Roeder RG. 2011. Role for Dpy-30 in ES cell-fate specification by regulation of H3K4 methylation within bivalent domains. *Cell* **144:** 513–525. doi:10.1016/j.cell.2011.01.020

Karolchik D, Kuhn RM, Baertsch R, Barber GP, Clawson H, Diekhans M, Giardine B, Harte RA, Hinrichs AS, Hsu F, et al. 2008. The UCSC Genome Browser Database: 2008 update. *Nucleic Acids Res* **36:** D773–D779. doi:10.1093/nar/gkm966

Kask P, Palo K, Ullmann D, Gall K. 1999. Fluorescence-intensity distribution analysis and its application in biomolecular detection technology. *Proc Natl Acad Sci* **96:** 13756–13761. doi:10.1073/pnas.96.24.13756

Kidder BL, Hu G, Zhao K. 2014. KDM5B focuses H3K4 methylation near promoters and enhancers during embryonic stem cell self-renewal and differentiation. *Genome Biol* **15:** R32. doi:10.1186/gb-2014-15-2-r32

Klein BJ, Piao L, Xi Y, Rincon-Arano H, Rothbart SB, Peng D, Wen H, Larson C, Zhang X, Zheng X, et al. 2014. The histone-H3K4-specific demethylase KDM5B binds to its substrate and product through distinct PHD fingers. *Cell Rep* **6:** 325–335. doi:10.1016/j.celrep.2013.12.021

Klose RJ, Kallin EM, Zhang Y. 2006. JmjC-domain-containing proteins and histone demethylation. *Nat Rev Genet* **7:** 715–727. doi:10.1038/nrg1945

Krogan NJ, Dover J, Khorrami S, Greenblatt JF, Schneider J, Johnston M, Shilatifard A. 2002. COMPASS, a histone H3 (Lysine 4) methyltransferase required for telomeric silencing of gene expression. *J Biol Chem* **277:** 10753–10755. doi:10.1074/jbc.C200023200

Kuang Z, Cai L, Zhang X, Ji H, Tu BP, Boeke JD. 2014. High-temporal-resolution view of transcription and chromatin states across distinct metabolic states in budding yeast. *Nat Struct Mol Biol* **21:** 854–863. doi:10.1038/nsmb.2881

Lee JE, Wang C, Xu S, Cho YW, Wang L, Feng X, Baldridge A, Sartorelli V, Zhuang L, Peng W, et al. 2013. H3K4 mono- and dimethyltransferase MLL4 is required for enhancer activation during cell differentiation. *eLife* **2:** e01503. doi:10.7554/eLife.01503

Lenstra TL, Benschop JJ, Kim T, Schulze JM, Brabers NACH, Margaritis T, van de Pasch LAL, van Heesch SAAC, Brok MO, Groot Koerkamp MJA, et al. 2011. The specificity and topology of chromatin interaction pathways in yeast. *Mol Cell* **42:** 536–549. doi:10.1016/j.molcel.2011.03.026

Li H, Durbin R. 2010. Fast and accurate long-read alignment with Burrows–Wheeler transform. *Bioinformatics* **26:** 589–595. doi:10.1093/bioinformatics/btp698

Li Y, Han J, Zhang Y, Cao F, Liu Z, Li S, Wu J, Hu C, Wang Y, Shuai J, et al. 2016. Structural basis for activity regulation of MLL family methyltransferases. *Nature* **530:** 447–452. doi:10.1038/nature16952

Liang G, Klose RJ, Gardner KE, Zhang Y. 2007. Yeast Jhd2p is a histone H3 Lys4 trimethyl demethylase. *Nat Struct Mol Biol* **14:** 243–245. doi:10.1038/nsmb1204

Logie C, Peterson CL. 1999. Purification and biochemical properties of yeast SWI/SNF complex. *Meth Enzymol* **304:** 726–741. doi:10.1016/S0076-6879(99)04044-6

Luger K, Mäder AW, Richmond RK, Sargent DF, Richmond TJ. 1997. Crystal structure of the nucleosome core particle at 2.8 Å resolution. *Nature* **389:** 251–260. doi:10.1038/38444

Margaritis T, Oreal V, Brabers N, Maestroni L, Vitaliano-Prunier A, Benschop JJ, van Hooff S, van Leenen D, Dargemont C, Géli V, et al. 2012. Two distinct repressive mechanisms for histone 3 lysine 4 methylation through promoting 3′-end antisense transcription. *PLoS Genet* **8:** e1002952. doi:10.1371/journal.pgen.1002952

McDowall MD, Harris MA, Lock A, Rutherford K, Staines DM, Bähler J, Kersey PJ, Oliver SG, Wood V. 2015. PomBase 2015: updates to the fission yeast database. *Nucleic Acids Res* **43:** D656–D661. doi:10.1093/nar/gku1040

Miller T, Krogan NJ, Dover J, Erdjument-Bromage H, Tempst P, Johnston M, Greenblatt JF, Shilatifard A. 2001. COMPASS: a complex of proteins associated with a trithorax-related SET domain protein. *Proc Natl Acad Sci* **98:** 12902–12907. doi:10.1073/pnas.231473398

Morillon A, Karabetsou N, Nair A, Mellor J. 2005. Dynamic lysine methylation on histone H3 defines the regulatory phase of gene transcription. *Mol Cell* **18:** 723–734. doi:10.1016/j.molcel.2005.05.009

Nagy PL, Griesenbeck J, Kornberg RD, Cleary ML. 2002. A trithorax-group complex purified from *Saccharomyces cerevisiae* is required for methylation of histone H3. *Proc Natl Acad Sci* **99:** 90–94. doi:10.1073/pnas.221596698

Newlon MG, Roy M, Morikis D, Hausken ZE, Coghlan V, Scott JD, Jennings PA. 1999. The molecular basis for protein kinase A anchoring revealed by solution NMR. *Nat Struct Biol* **6:** 222–227. doi:10.1038/6663

Ng HH, Robert F, Young RA, Struhl K. 2003. Targeted recruitment of Set1 histone methylase by elongating Pol II provides a localized mark and memory of recent transcriptional activity. *Mol Cell* **11:** 709–719. doi:10.1016/S1097-2765(03)00092-3

Nishimura K, Fukagawa T, Takisawa H, Kakimoto T, Kanemaki M. 2009. An auxin-based degron system for the rapid depletion of proteins in nonplant cells. *Nat Methods* **6:** 917–922. doi:10.1038/nmeth.1401

Pelechano V, Chávez S, Pérez-Ortín JE. 2010. A complete set of nascent transcription rates for yeast genes. *PLoS One* **5:** e15442. doi:10.1371/journal.pone.0015442

Qu Q, Takahashi YH, Yang Y, Hu H, Zhang Y, Brunzelle JS, Couture JF, Shilatifard A, Skiniotis G. 2018. Structure and conformational dynamics of a COMPASS histone H3K4 methyltransferase complex. *Cell* **174:** 1117–1126.e12. doi:10.1016/j.cell.2018.07.020

Radman-Livaja M, Liu CL, Friedman N, Schreiber SL, Rando OJ. 2010. Replication and active demethylation represent partially overlapping mechanisms for erasure of H3K4me3 in budding yeast. *PLoS Genet* **6:** e1000837. doi:10.1371/journal.pgen.1000837

Ramachandran S, Zentner GE, Henikoff S. 2015. Asymmetric nucleosomes flank promoters in the budding yeast genome. *Genome Res* **25:** 381–390. doi:10.1101/gr.182618.114

Ramakrishnan S, Pokhrel S, Palani S, Pflueger C, Parnell TJ, Cairns BR, Bhaskara S, Chandrasekharan MB. 2016. Counteracting H3K4 methylation modulators Set1 and Jhd2 co-regulate chromatin dynamics and gene transcription. *Nat Commun* **7:** 11949. doi:10.1038/ncomms11949

Ramírez F, Dündar F, Diehl S, Grüning BA, Manke T. 2014. deepTools: a flexible platform for exploring deep-sequencing data. *Nucleic Acids Res* **42:** W187–W191. doi:10.1093/nar/gku365

Rao RC, Dou Y. 2015. Hijacked in cancer: the KMT2 (MLL) family of methyltransferases. *Nat Rev Cancer* **15:** 334–346. doi:10.1038/nrc3929

Rhee HS, Bataille AR, Zhang L, Pugh BF. 2014. Subnucleosomal structures and nucleosome asymmetry across a genome. *Cell* **159:** 1377–1388. doi:10.1016/j.cell.2014.10.054

Roguev A, Schaft D, Shevchenko A, Pijnappel WW, Wilm M, Aasland R, Stewart AF. 2001. The *Saccharomyces cerevisiae* Set1 complex includes an Ash2 homologue and methylates histone 3 lysine 4. *EMBO J* **20:** 7137–7148. doi:10.1093/emboj/20.24.7137

Roguev A, Schaft D, Shevchenko A, Aasland R, Shevchenko A, Stewart AF. 2003. High conservation of the Set1/Rad6 axis of histone 3 lysine 4 methylation in budding and fission yeasts. *J Biol Chem* **278:** 8487–8493. doi:10.1074/jbc.M209562200

Ruthenburg AJ, Allis CD, Wysocka J. 2007. Methylation of lysine 4 on histone H3: intricacy of writing and reading a single epigenetic mark. *Mol Cell* **25:** 15–30. doi:10.1016/j.molcel.2006.12.014

Santos-Rosa H, Kirmizis A, Nelson C, Bartke T, Saksouk N, Cote J, Kouzarides T. 2009. Histone H3 tail clipping regulates gene expression. *Nat Struct Mol Biol* **16:** 17–22. doi:10.1038/nsmb.1534

Scandaglia M, Lopez-Atalaya JP, Medrano-Fernandez A, Lopez-Cascales MT, Del Blanco B, Lipinski M, Benito E, Olivares R, Iwase S, Shi Y, et al. 2017. Loss of Kdm5c causes spurious transcription and prevents the fine-tuning of activity-regulated enhancers in neurons. *Cell Rep* **21:** 47–59. doi:10.1016/j.celrep.2017.09.014

Schmitz SU, Albert M, Malatesta M, Morey L, Johansen JV, Bak M, Tommerup N, Abarrategui I, Helin K. 2011. Jarid1b targets genes regulating development and is involved in neural differentiation. *EMBO J* **30:** 4586–4600. doi:10.1038/emboj.2011.383

Seward DJ, Cubberley G, Kim S, Schonewald M, Zhang L, Tripet B, Bentley DL. 2007. Demethylation of trimethylated histone H3 Lys4 in vivo by JARID1 JmjC proteins. *Nat Struct Mol Biol* **14:** 240–242. doi:10.1038/nsmb1200

Shema E, Jones D, Shoresh N, Donohue L, Ram O, Bernstein BE. 2016. Single-molecule decoding of combinatorially modified nucleosomes. *Science* **352:** 717–721. doi:10.1126/science.aad7701

Shi X, Kachirskaia I, Walter KL, Kuo JHA, Lake A, Davrazou F, Chan SM, Martin DGE, Fingerman IM, Briggs SD, et al. 2007. Proteome-wide analysis in *Saccharomyces cerevisiae* identifies several PHD fingers as novel direct and selective binding modules of histone H3 methylated at either lysine 4 or lysine 36. *J Biol Chem* **282:** 2450–2455. doi:10.1074/jbc.C600286200

Soares LM, He PC, Chun Y, Suh H, Kim T, Buratowski S. 2017. Determinants of histone H3K4 methylation patterns. *Mol Cell* **68:** 773–785. doi:10.1016/j.molcel.2017.10.013

South PF, Fingerman IM, Mersman DP, Du HN, Briggs SD. 2010. A conserved interaction between the SDI domain of Bre2 and the Dpy-30 domain of Sdc1 is required for histone methylation and gene expression. *J Biol Chem* **285:** 595–607. doi:10.1074/jbc.M109.042697

Torres IO, Kuchenbecker KM, Nnadi CI, Fletterick RJ, Kelly MJS, Fujimori DG. 2015. Histone demethylase KDM5A is regulated by its reader domain through a positive-feedback mechanism. *Nat Commun* **6:** 364. doi:10.1038/ncomms7204

Trapnell C, Pachter L, Salzberg SL. 2009. TopHat: discovering splice junctions with RNA-seq. *Bioinformatics* **25:** 1105–1111. doi:10.1093/bioinformatics/btp120

Trapnell C, Williams BA, Pertea G, Mortazavi A, Kwan G, van Baren MJ, Salzberg SL, Wold BJ, Pachter L. 2010. Transcript assembly and quantification by RNA-seq reveals unannotated transcripts and isoform switching during cell differentiation. *Nat Biotechnol* **28:** 511–515. doi:10.1038/nbt.1621

Trapnell C, Roberts A, Goff L, Pertea G, Kim D, Kelley DR, Pimentel H, Salzberg SL, Rinn JL, Pachter L. 2012. Differential gene and transcript expression analysis of RNA-seq experiments with TopHat and Cufflinks. *Nat Protoc* **7:** 562–578. doi:10.1038/nprot.2012.016

Trapnell C, Hendrickson DG, Sauvageau M, Goff L, Rinn JL, Pachter L. 2013. Differential analysis of gene regulation at transcript resolution with RNA-seq. *Nat Biotechnol* **31:** 46–53. doi:10.1038/nbt.2450

Tremblay V, Zhang P, Chaturvedi CP, Thornton J, Brunzelle JS, Skiniotis G, Shilatifard A, Brand M, Couture JF. 2014. Molecular basis for DPY-30 association to COMPASS-like and NURF complexes. *Structure* **22:** 1821–1830. doi:10.1016/j.str.2014.10.002

Trésaugues L, Dehé PM, Guérois R, Rodriguez-Gil A, Varlet I, Salah P, Pamblanco M, Luciano P, Quevillon-Cheruel S, Sollier J, et al. 2006. Structural characterization of Set1 RNA recognition motifs and their role in histone H3 lysine 4 methylation. *J Mol Biol* **359:** 1170–1181. doi:10.1016/j.jmb.2006.04.050

Tu BP, Kudlicki A, Rowicka M, McKnight SL. 2005. Logic of the yeast metabolic cycle: temporal compartmentalization of cellular processes. *Science* **310:** 1152–1158. doi:10.1126/science.1120499

Tu S, Bulloch EMM, Yang L, Ren C, Huang WC, Hsu PH, Chen CH, Liao CL, Yu HM, Lo WS, et al. 2007. Identification of histone demethylases in *Saccharomyces cerevisiae*. *J Biol Chem* **282:** 14262–14271. doi:10.1074/jbc.M609900200

van Rossum B, Fischle W, Selenko P. 2012. Asymmetrically modified nucleosomes expand the histone code. *Nat Struct Mol Biol* **19:** 1064–1066. doi:10.1038/nsmb.2433

Vermeulen M, Mulder KW, Denissov S, Pijnappel WWMP, van Schaik FMA, Varier RA, Baltissen MPA, Stunnenberg HG, Mann M, Timmers HTM. 2007. Selective anchoring of TFIID to nucleosomes by trimethylation of histone H3 lysine 4. *Cell* **131:** 58–69. doi:10.1016/j.cell.2007.08.016

Vermeulen M, Eberl HC, Matarese F, Marks H, Denissov S, Butter F, Lee KK, Olsen JV, Hyman AA, Stunnenberg HG, et al. 2010. Quantitative interaction proteomics and genome-wide profiling of epigenetic histone marks and their readers. *Cell* **142:** 967–980. doi:10.1016/j.cell.2010.08.020

Voigt P, LeRoy G, Drury WJ, Zee BM, Son J, Beck DB, Young NL, Garcia BA, Reinberg D. 2012. Asymmetrically modified nucleosomes. *Cell* **151:** 181–193. doi:10.1016/j.cell.2012.09.002

Voigt P, Tee WW, Reinberg D. 2013. A double take on bivalent promoters. *Genes Dev* **27:** 1318–1338. doi:10.1101/gad.219626.113

Wang X, Lou Z, Dong X, Yang W, Peng Y, Yin B, Gong Y, Yuan J, Zhou W, Bartlam M, et al. 2009. Crystal structure of the C-terminal domain of human DPY-30-like protein: a component of the histone methyltransferase complex. *J Mol Biol* **390:** 530–537. doi:10.1016/j.jmb.2009.05.061

Weiner A, Chen HV, Liu CL, Rahat A, Klien A, Soares L, Gudipati M, Pfeffner J, Regev A, Buratowski S, et al. 2012. Systematic dissection of roles for chromatin regulators in a yeast stress response. *PLoS Biol* **10:** e1001369. doi:10.1371/journal.pbio.1001369

Woo H, Dam Ha S, Lee SB, Buratowski S, Kim T. 2017. Modulation of gene expression dynamics by co-transcriptional histone methylations. *Exp Mol Med* **49:** e326. doi:10.1038/emm.2017.19

Zhang Y, Yang H, Guo X, Rong N, Song Y, Xu Y, Lan W, Zhang X, Liu M, Xu Y, et al. 2014. The PHD1 finger of KDM5B recognizes unmodified H3K4 during the demethylation of histone H3K4me2/3 by KDM5B. *Protein Cell* **5:** 837–850. doi:10.1007/s13238-014-0078-4

Zhang H, Li M, Gao Y, Jia C, Pan X, Cao P, Zhao X, Zhang J, Chang W. 2015a. Structural implications of Dpy30 oligomerization for MLL/SET1 COMPASS H3K4 trimethylation. *Protein Cell* **6:** 147–151. doi:10.1007/s13238-014-0127-z

Zhang P, Chaturvedi CP, Tremblay V, Cramet M, Brunzelle JS, Skiniotis G, Brand M, Shilatifard A, Couture JF. 2015b. A phosphorylation switch on RbBP5 regulates histone H3 Lys4 methylation. *Genes Dev* **29:** 123–128. doi:10.1101/gad.254870.114